



The effect of external perturbations on nonlinear panel flutter at low supersonic speed

Anastasia Shishaeva^{a,*}, Andrey Aksenov^b, Vasily Vedeneev^a

^a Lomonosov Moscow State University, 1, Leninskie Gory, Moscow, Russia

^b Joint Institute for High Temperatures of the Russian Academy of Sciences, Izhorskaya st. 13 Bd.2, Moscow, Russia



ARTICLE INFO

Article history:

Received 2 August 2021

Received in revised form 30 January 2022

Accepted 24 March 2022

Available online xxxx

Keywords:

Panel flutter

Low supersonic flow

External disturbance

Hysteresis

Flow control

ABSTRACT

We studied two-dimensional nonlinear flutter oscillations of a flat elastic panel in a low supersonic flow, where several panel eigenmodes are simultaneously unstable, and resulting nonlinear oscillations are governed by the nonlinear interaction of growing modes. The objective of our work was to study the dependence of limit cycle oscillations of the panel on an external disturbance. To analyse possible limit cycle oscillations, we first investigated the effect of the spatial distribution and amplitude of the initial excitation loading. We show that, depending on the initial perturbation, different modes of limit cycle oscillations can develop, in which the cyclic stress amplitude differs by an order of magnitude. Second, we investigated the effect of a short strong perturbation applied to the developed limit cycle oscillations and show the possibility of switching the limit cycle mode from high- to low-energy oscillations, thus providing the ability to control oscillations of the fluttering panel.

© 2022 Elsevier Ltd. All rights reserved.

1. Introduction

Flutter of skin panels is a well-known aeroelastic phenomenon occurring at transonic and supersonic flight speeds. After its first manifestation in the 1940s, it was intensely studied from the 1950s to 70s, both in linear and nonlinear formulations (Bolotin, 1963; Grigolyuk et al., 1965; Dowell, 1975; Novichkov, 1978; Mei et al., 1999; Algazin and Kiiko, 2006). The common feature of most of those studies is the use of a simplified aerodynamic model, piston theory, which accurately predicts unsteady aerodynamic loading at high supersonic Mach numbers, $M > 2$, including hypersonic speeds where real-gas effects are manifested (Vedeneev and Nesterov, 2019), and which is suitable also for non-flat skin panels and cylindrical shells (Amabili and Pellicano, 2001, 2002).

Although a few earlier studies (Dowell, 1967, 1973) also included lower Mach numbers that require more general aerodynamic theories, either potential flow or linearized Navier–Stokes equations, significant progress in transonic and low supersonic panel flutter was achieved in the 21st century. Besides the coupled-mode flutter mechanism typical for high supersonic speed, a different, single-mode flutter mechanism exists at lower flight speeds, which essentially enlarges the total region of instability in the parameter space (Vedeneev, 2012, 2013a; Shitov and Vedeneev, 2017). The difference in the flutter mechanism also yields a much more significant response of aeroelastic instability to the boundary layer over the panel at low supersonic speeds (Muhlstein et al., 1968; Gaspers et al., 1970; Hashimoto et al., 2009; Vedeneev, 2013b; Alder, 2015; Bondared and Vedeneev, 2016, 2017, 2018). A series of nonlinear studies (Dowell, 1967; Bendiksen

* Corresponding author.

E-mail addresses: anastasiashishaeva@rambler.ru (A. Shishaeva), andrey@tesis.com.ru (A. Aksenov), vasily@vedeneev.ru (V. Vedeneev).

URLs: <https://www.flowvision.ru> (A. Aksenov), <https://www.vedeneev.ru> (V. Vedeneev).

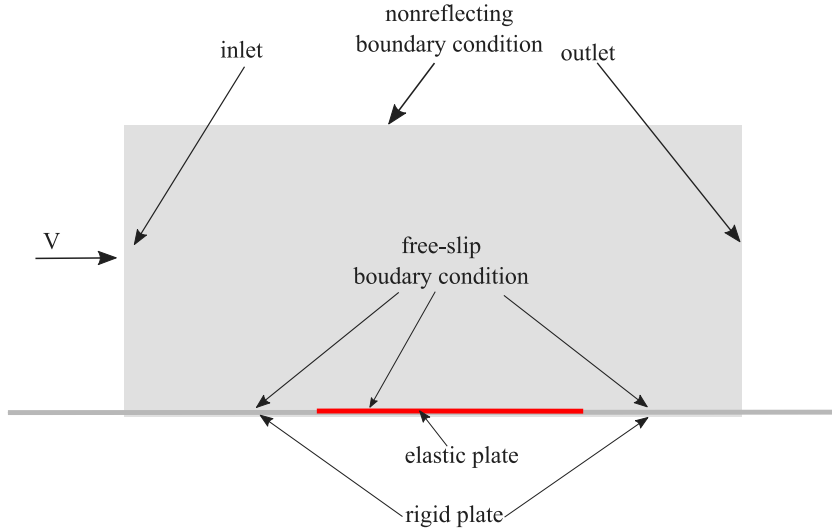


Fig. 1. Simulation domain.

and Davis, 1995; Gordnier and Visbal, 2002; Mei et al., 2014; Shishaeva et al., 2015; Alder, 2015, 2016; Hejranfar and Azampour, 2016; Zhou et al., 2021) revealed that the amplitude, frequency, and flutter mode shape change essentially when the Mach number crosses $M \approx \sqrt{2}$, because the flutter mechanism is switched from single-mode to coupled-mode or vice versa. Recently, growing interest has emerged in nonlinear flutter oscillations of curved panels at transonic and supersonic speeds, either due to initial curvature (Mei et al., 2017; Bhatia and Beran, 2018; An et al., 2020), or due to interaction with the impinging shock wave (Willems et al., 2013; Visbal, 2013; Boyer et al., 2018; Shinde et al., 2019).

In most previous studies, nonlinear transonic panel flutter occurred in the first natural mode of the panel. It is known, however, that, in contrast to coupled-mode flutter, where only one eigenmode (being the mixture of the first and the second panel natural modes) is unstable, multiple natural modes are linearly unstable with respect to single-mode flutter (Vedeneev, 2012, 2013a; Shitov and Vedeneev, 2017). Accordingly, theoretical nonlinear analysis predicts several different stable limit cycles (Vedeneev, 2007, 2013c): some correspond to oscillations in one certain mode, and the others to multiple-mode oscillations, being either independent, or oscillating in the regime of internal resonance. The existence of multiple limit cycles was partially confirmed in the direct time-domain simulations (Gordnier and Visbal, 2002; Alder, 2015; Shishaeva et al., 2015; Hejranfar and Azampour, 2016; Shishaeva et al., 2018), where the excitation of a panel by different initial loading yielded the development of different limit cycles. However, higher-mode limit cycles predicted theoretically were excited in numerical calculations only at certain isolated parameter values so that their existence and stability at a wider range of parameters remains under question. Their analysis is the goal of this study.

In Section 2, we briefly formulate the problem and describe the method of solution; Section 3 reviews the results obtained previously with a small-amplitude initial perturbation. Calculation results for large-amplitude perturbations are presented and discussed in Section 4. We show that higher-mode limit cycles are perfectly excited but are very different in terms of the total energy of oscillations (and, hence, in terms of fatigue lifetime). The question then is whether it is possible to control the limit cycle, that is, to switch from a higher-mode high-energy limit cycle to a lower-mode limit cycle by introducing a perturbation into already developed limit cycle oscillations. This question is analysed in Section 5. Finally, Section 6 summarizes the results and concludes the paper.

2. Formulation of the problem and method of solution

The problem formulation is standard for two-dimensional panel flutter analysis: we considered a clamped flat elastic plate mounted into a rigid plane and exposed to a supersonic air flow, as shown in Fig. 1. The numerical model is similar to the one used in Shishaeva et al. (2015, 2018). The computational domain of the flow is large enough to exclude the influence of the top boundary on the plate dynamics, which was checked in a convergence study. The air is modelled as inviscid perfect gas. We did not take viscosity and turbulence into account, assuming that the boundary layer is thin and does not affect aeroelastic stability (more specifically, Navier–Stokes equations were solved, but the viscosity was set sufficiently small to not affect the motion, and the independence from the viscosity value was separately checked). In connection with this assumption, a free-slip boundary condition was set on the plate surface. At the inlet (left boundary), the following parameters were set: pressure $P_\infty = 10^5$ Pa, temperature $T_\infty = 273$ K, and velocity v directed parallel to the plate and specified according to Mach number M within the range $1 < M < 2$. A non-reflecting boundary condition was set on the top boundary, and the same inlet parameters were employed to calculate Riemann invariants. At the outlet (right boundary), no boundary conditions were specified due to the supersonic flow speed.

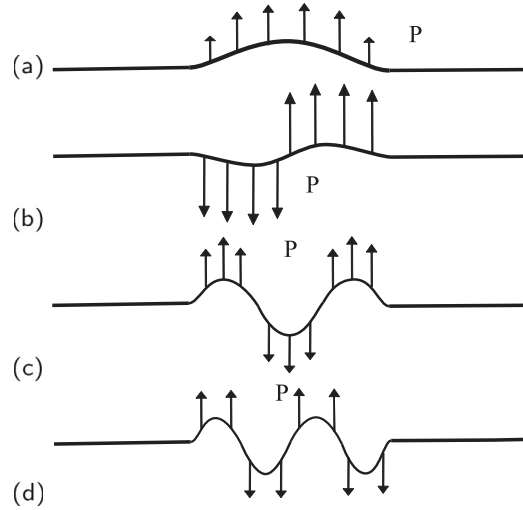


Fig. 2. Initial perturbation in the form of the first (a), second (b), third (c), and fourth (d) natural modes.

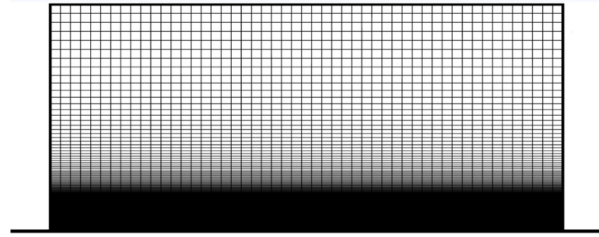


Fig. 3. Computational grid of the flow domain.

The plate is geometrically nonlinear and obeys a Mindlin shell theory, which allows through-the-thickness shear deformation. Bending strain tensor is the approximation of the Koiter–Sanders theory (Dassault Systèmes, 2012, §3.6.1, §3.6.5), originally developed for the classical shell theory (Budiansky and Sanders, 1962; Amabili, 2008). The plate has length $L = 0.3$ m and thickness $h = 0.001$ m; Young's modulus $E = 2 \times 10^{11}$ Pa, Poisson's coefficient $\nu = 0.3$, and density $\rho = 7800$ kg/m³ represent material properties of steel. As well as in Shishaeva et al. (2015, 2018), in dimensionless terms, these parameters are equivalent to an aluminium plate in air at 11,000 m above sea level. The air pressure perturbation acts on the top surface of the plate and a zero stress is set at the bottom surface.

In this study, since we consider constant inlet pressure and temperature, and only velocity is varied, all dimensionless parameters common in panel flutter studies are expressed through the Mach number, namely

$$\lambda^* = \frac{\rho_a v^2 L^3}{D} = 206 \times M^2, \quad \mu^* = \frac{\rho_a L}{\rho h} = 0.049,$$

where λ^* is dimensionless dynamic pressure, and μ^* is mass ratio; $\rho_a = 1.28$ kg/m³ is the air density, $v = Ma$ is the air speed, $a = 331.2$ m/s is the speed of sound, and $D = Eh^3/(12(1 - \nu^2))$ is the plate bending stiffness. In what follows, we will use the Mach number as an indication of the regime so that λ^* and μ^* can be calculated through the expressions above. In the series of calculations, the velocity is changed with a step $\Delta v = 10$ m/s, which corresponds to $\Delta M = 0.03$. The calculations' results will be presented in a dimensionless form: deflections are nondimensionalized by h , and time by L/a .

The panel–flow system is disturbed by a short ($\Delta t = 10^{-4}$ s) initial perturbation in the form of a specified pressure distribution over the panel, whose intensity is characterized by the dimensionless parameter $P = P_d/P_\infty$, where P_d is the dimensional pressure amplitude. We considered initial perturbations that excite the first, second, third, or fourth natural modes, which differ in the spatial distribution of applied pressure (Fig. 2). We checked that panel oscillations in a vacuum caused by each of the perturbations were very close to pure oscillations with the corresponding natural mode shape and frequency.

After applying the perturbation, the coupled plate–flow dynamics was calculated in two commercial codes: FlowVision (air motion) and Abaqus (plate motion). Both solvers were two-way coupled through the direct coupling algorithm (Aksenov et al., 2008). The flow mesh is shown in Fig. 3, its size was 50×494 control volumes. The volume size was

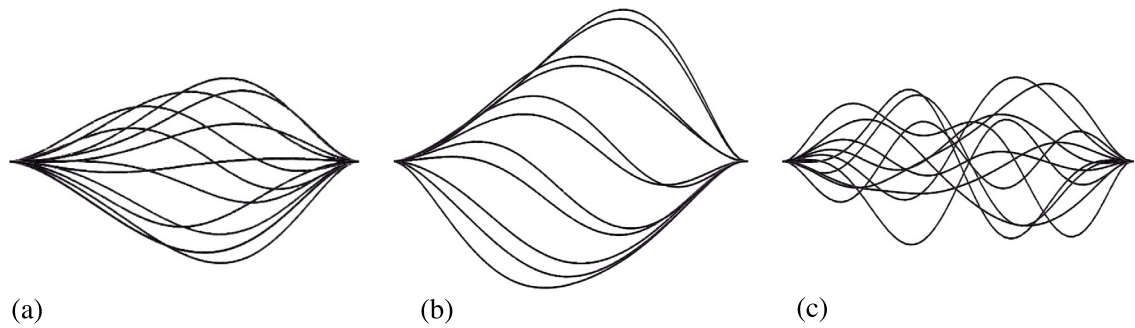


Fig. 4. Snapshots of the plate shape at the first-mode LCOs (a), resonant LCOs (b), and non-periodic oscillations (c), vertical scale 50:1.

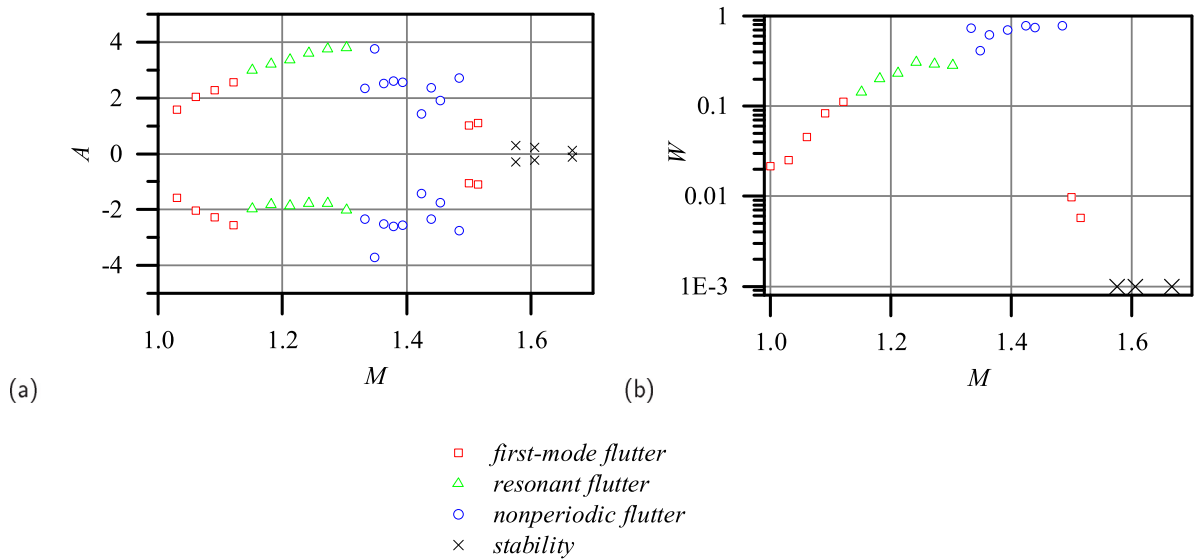


Fig. 5. Reference point amplitude (a) and the total plate energy (b) of the LCOs after a small disturbance ($P = 0.1$) vs. Mach number.

decreasing towards the panel in order to have the near-panel elements sufficiently small to accurately capture the panel motion caused by the initial perturbation. The panel mesh consists of 60 continuum shell elements. Validation of the numerical model, including the convergence study in mesh size, time step, and the flow domain size, is described in Shishaeva et al. (2015) and omitted here for the sake of brevity.

3. Previous results for small-amplitude perturbations

In our previous study (Shishaeva et al., 2015), we considered the development of nonlinear panel flutter oscillations at constant subsonic, transonic, and supersonic speeds under a small external disturbance with the amplitude $P = 0.1$. We detected several forms of the nonlinear development of instability at different Mach numbers. The first was static divergence that occurred for $0.7 < M < 1$. The second was the first-mode flutter (Fig. 4a) developing at $1 < M \leq 1.12$ and $1.5 \leq M < 1.54$. Note that for $M \geq 1.54$ the amplitude was less than 0.1, which can be considered ‘almost’ stable state. The third was a 2:1 resonant flutter in the range $1.15 \leq M \leq 1.30$ (Fig. 4b). It differed from single-mode limit cycles in that it was not symmetric (displacement upward was larger than downward) and a doubled frequency was present in the frequency spectrum, signifying the presence of both the first and second modes being in internal 2:1 resonance. The last one was non-periodic, irregular higher-mode oscillations that occurred for $1.33 \leq M < 1.5$ (Fig. 4c). The plate was stable for $1.54 \leq M < M_{cr}$, where $M_{cr} = 2.92$ is the critical Mach number of the coupled-mode flutter for the parameters considered. It was also found that, by applying a strong initial first-mode perturbation in the range of Mach numbers, where small-amplitude perturbation developed into the resonant flutter, a different limit cycle purely in the shape of the first-mode developed, which aligned with the theoretically expected coexistence of these two limit cycles (Vedenev, 2013c).

The plot of a reference point amplitude (the point was located at 0.22 m downstream of the leading plate edge, which was approximately 3/4 of the plate length) is shown in Fig. 5a. The amplitude grew with the increase of the Mach

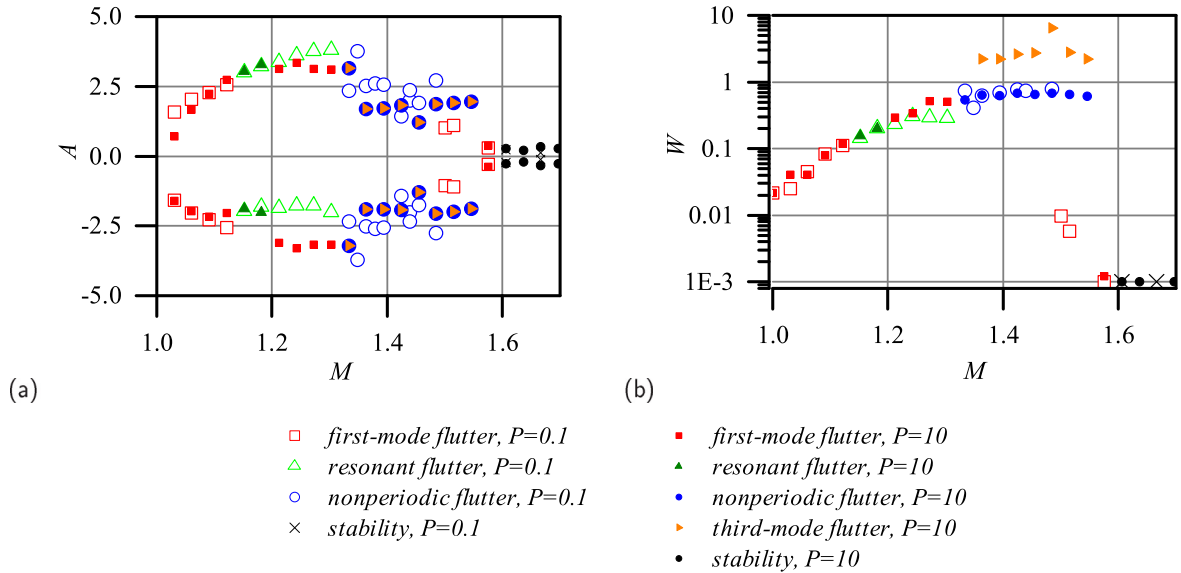


Fig. 6. Amplitude of the control point (a) and energy of the plate (b) under the small ($P = 0.1$) disturbance and strong first-mode ($P = 10$) disturbance vs. Mach number.

number while passing the region of the first-mode and resonant flutter, $1 < M \leq 1.3$ (red squares and green triangles), decreased in the regime of non-periodic flutter for $1.33 \leq M \leq 1.48$ (blue circles), and decayed in the area of the first-mode flutter for $1.5 \leq M \leq 1.515$ (red squares). The typical amplitude of the resonant flutter was the largest among oscillation modes. However, from the point of view of fatigue strength, strain or stress amplitude or total plate energy are more adequate characteristics of the severity of oscillations, because higher-mode oscillations of the same or even lower deflection amplitude have larger stress amplitude and total energy, which means a shorter fatigue lifetime. This is why, in the present study, we have considered total plate energy and oscillation mode as characteristics of limit cycle oscillations. The total energy was calculated as a sum of the kinetic (W_k) and strain energy (W_{str}) of the plate averaged over the full period of oscillations after their development. In a dimensionless form, it reads as $W = (W_k + W_{str})/(\rho_a a^2 Lh/2)$.

Fig. 5b shows the dimensionless total energy for the same limit cycle oscillations as in Fig. 5a. The energy of non-periodic flutter oscillations was significantly higher than of resonant flutter, which was caused by shorter bending wavelength, and, consequently, larger dynamic strain and stress. This means that the non-periodic flutter is the most dangerous type of nonlinear oscillations developed after applying a small-amplitude perturbation. We expect that limit cycle oscillations in higher modes would correspond to the same or larger energy, i.e., they are the most severe for the fatigue strength. Although predicted theoretically (Vedenev, 2013c), such limit cycles were rarely observed in calculations with a small initial perturbation. The next section is devoted to their excitation and analysis in a wide range of Mach numbers by means of large-amplitude perturbations.

4. The panel dynamics after large-amplitude perturbations

4.1. The first-mode disturbance

Let us consider the development of the first-mode initial perturbation with the amplitude $P = 10$, i.e., 100 times stronger than considered before (Fig. 6). Three types of the plate dynamics were observed. The first-mode flutter occurred for $1 < M \leq 1.12$, $1.21 \leq M \leq 1.3$ and at $M = 1.575$. The resonant flutter was observed in a short range of Mach numbers $1.15 \leq M \leq 1.18$. Finally, for $1.33 \leq M \leq 1.54$, a sequence of two limit dynamics took place: first, high-frequency non-periodic oscillations developed, which were similar to those developed after a small-amplitude perturbation for $1.33 \leq M \leq 1.42$ (Shishaeva et al., 2015). After a certain period, they transformed into the third-mode limit cycle oscillations, as shown in Fig. 7: although other mode components were visible due to their linear instability, the dominance of the third mode was clear. Despite the displacement amplitude of the reference point not changing in the transition from non-periodic to third-mode oscillations, the plate energy increased more than three times. The amplitude became very small at $M > 1.575$ when the oscillations returned to the first-mode, and the plate was fully stabilized at $M = 1.6$.

Comparing the plate dynamics for small ($P = 0.1$) and strong ($P = 10$) first-mode perturbations, we saw two changes. First, when increasing the Mach number for strong perturbation, the first-mode LCOs developed at $1.21 \leq M \leq 1.3$, where resonant LCOs occur for small perturbation (Fig. 6). The reason was discussed in Shishaeva et al. (2015): after a small perturbation, initially, first-mode limit oscillations grow. As the frequency of nonlinear oscillations increased

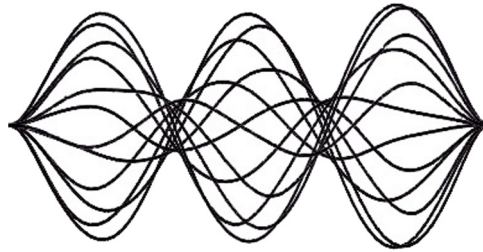


Fig. 7. Snapshots of the plate shape at the third-mode LCO (vertical scale 50:1).

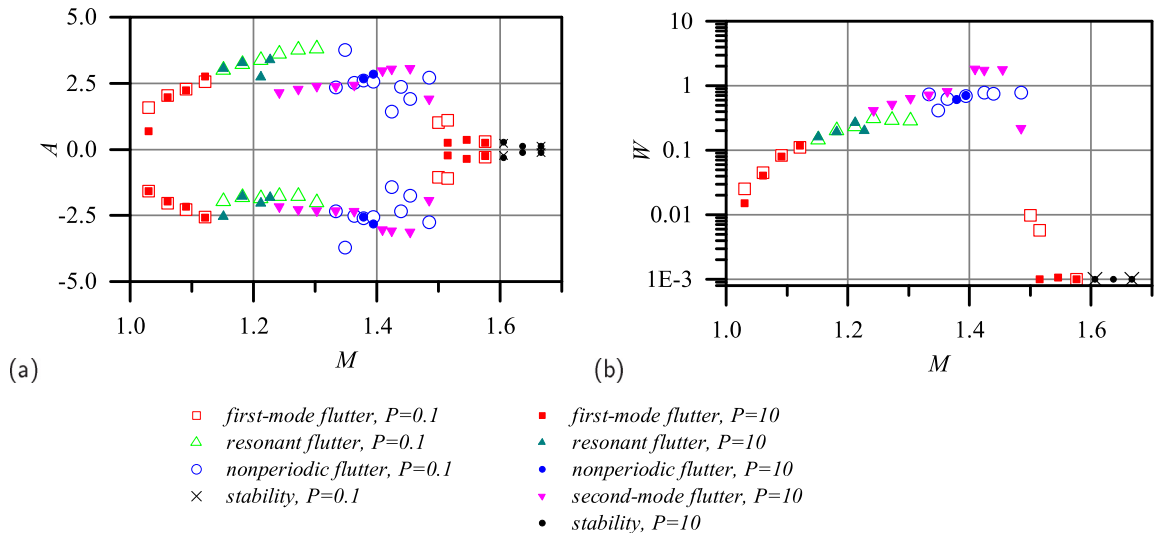


Fig. 8. Amplitude of the control point (a) and energy of the plate (b) under the small ($P = 0.1$) disturbance and strong second-mode ($P = 10$) disturbance vs. Mach number.

following the amplitude, at some moment, the second-mode frequency became proportional to the first-mode frequency, and internal 2:1 resonance occurred. After the resonant lock-in, both modes grew in amplitude until the energy balance was achieved (energy obtained by the plate from the flow through the first mode equals the energy dissipated to the flow through the second mode), and the resonant limit cycle formed. A strong initial perturbation resulted in bypassing the moment of resonant lock, and the first-mode limit cycle oscillations formed. As seen in Fig. 6b, the plate energy of the first-mode oscillations was higher than of the resonant flutter, i.e., the latter was more favourable for the fatigue stress. In the Mach number range $1.33 \leq M \leq 1.42$, where non-periodic oscillations developed in both cases, plate energies were close, but amplitudes were different. The development of the third-mode limit cycle (observed only in the case of strong perturbation) resulted in several times larger energy, i.e. this limit cycle was more destructive than non-periodic oscillations. Third-mode oscillations continued until the plate stabilization, without interruption of other oscillation types.

4.2. The second-mode disturbance

In this section, we analyse the effect of the second-mode strong disturbance (Fig. 8). As in the first-mode disturbance, there were four types of limit plate dynamics, but the third-mode limit cycle was not observed; instead, the second-mode limit cycle developed. Namely, the first-mode flutter occurred for $1 < M \leq 1.12$ and $1.51 \leq M \leq 1.57$, and the resonant 2:1 flutter for $1.15 \leq M \leq 1.22$. The second-mode LCOs were developed in the ranges $1.22 \leq M \leq 1.36$ and $1.4 \leq M \leq 1.5$, whose shape is shown in Fig. 9. Non-periodic oscillations were developed only in a short range of $1.38 \leq M \leq 1.39$. The point $M = 1.22$ was exceptional: first, the second-mode limit cycle was developed, but it appeared to be not sufficiently stable so that, after a certain period of time, the oscillations transformed into resonant LCOs.

As the same types of LCOs were developed for both first- and second-mode perturbations at $1 \leq M \leq 1.22$, the amplitude and the energy were the same. Then, for $M \geq 1.22$, the second-mode LCOs energy is larger than the resonant LCO energy developed after a small perturbation. Energies became equal again in the region of non-periodic oscillations, $1.38 \leq M \leq 1.39$. When oscillations were returned to the second mode, for $1.4 \leq M \leq 1.45$, the oscillation energy was two times higher for the same type of limit cycle at $1.22 \leq M \leq 1.36$. However, with the further increase of Mach

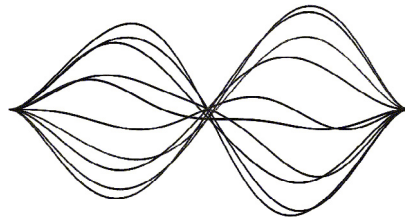


Fig. 9. The plate shape at the second-mode flutter (vertical scale 50:1).

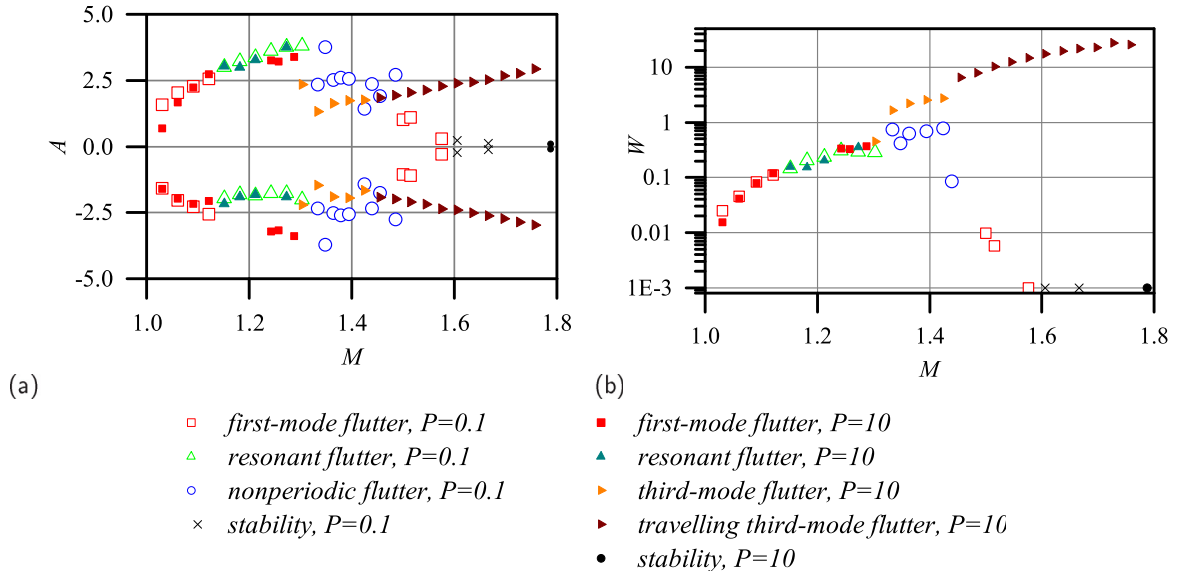


Fig. 10. Amplitude of the control point (a) and energy of the plate (b) under the small ($P = 0.1$) disturbance and strong third-mode ($P = 10$) disturbance vs. Mach number.

number, $M \geq 1.48$, the energy of the second-mode oscillations sharply decreases, although being larger than for the first-mode oscillations developed after a small-amplitude perturbation.

4.3. The third-mode disturbance

Now, consider the plate dynamics after applying large-amplitude third-mode perturbation (Fig. 10). As before, it resulted in the first-mode LCOs for $1 \leq M \leq 1.12$, for $1.24 \leq M \leq 1.26$, and for $M = 1.29$. The resonant LCOs were observed for $1.15 \leq M \leq 1.21$ and for $M = 1.27$. These ranges of different limit cycles were close to those excited by strong first-mode perturbation. This is in agreement with linear flutter boundaries: the third mode lost stability at a larger Mach number than the first-mode (Vedenev, 2012, 2013a). Although the third mode became linearly growing at $M \approx 1.14$ (Vedenev, 2013a), in the case of multiple growing modes, this did not immediately yield the existence of the corresponding stable limit cycle (Vedenev, 2013c): as the first and the second modes were also linearly growing, the third-mode limit cycle stays unstable, and the third-mode perturbation develops into the first- or resonant first- and second-mode oscillations. This situation continued while $M < 1.3$. For $1.3 \leq M \leq 1.44$, standing-wave third-mode LCOs were developed (Fig. 11a), signifying the existence and stability of this limit cycle. For larger Mach numbers, $1.45 \leq M \leq 1.75$, regular third-mode oscillations continued but with a sharply increased travelling-wave component (Fig. 11b). For brevity, we will call this oscillation regime travelling-wave flutter.

The oscillation energy was similar to that observed after the small-amplitude perturbation for $1 < M \leq 1.29$. Even when limit cycles were different, the amplitudes were also close, except for downward amplitude at $1.24 \leq M \leq 1.26$ and $M = 1.29$, where strong third-mode perturbation resulted in the first-mode LCOs, but small-amplitude perturbation results in the resonant LCOs (Fig. 10a). When the third-mode LCOs developed at $1.3 \leq M \leq 1.75$, the plate energy became significantly larger (Fig. 10b). Note that, when the standing wave was changed by a travelling one, the energy grew even more, despite the deflection amplitude continuously following its trend.

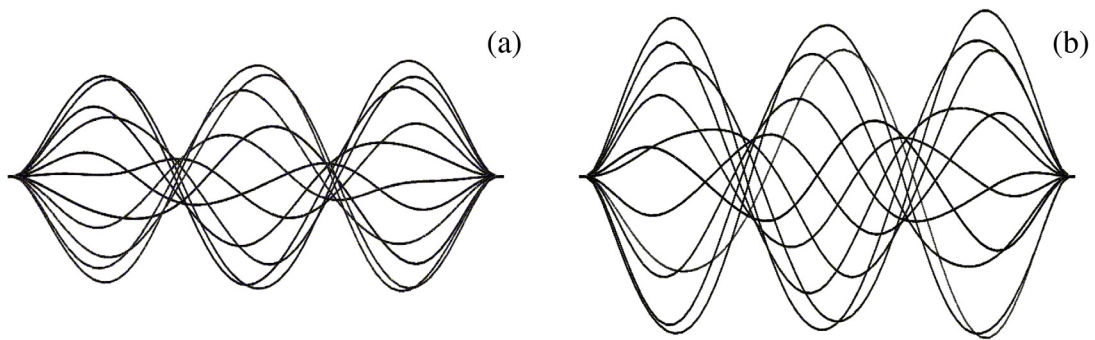


Fig. 11. The plate shape at the third-mode flutter in the form of standing wave at $M = 1.33$ (a) and travelling wave at $M = 1.45$ (b) (vertical scale 50:1).

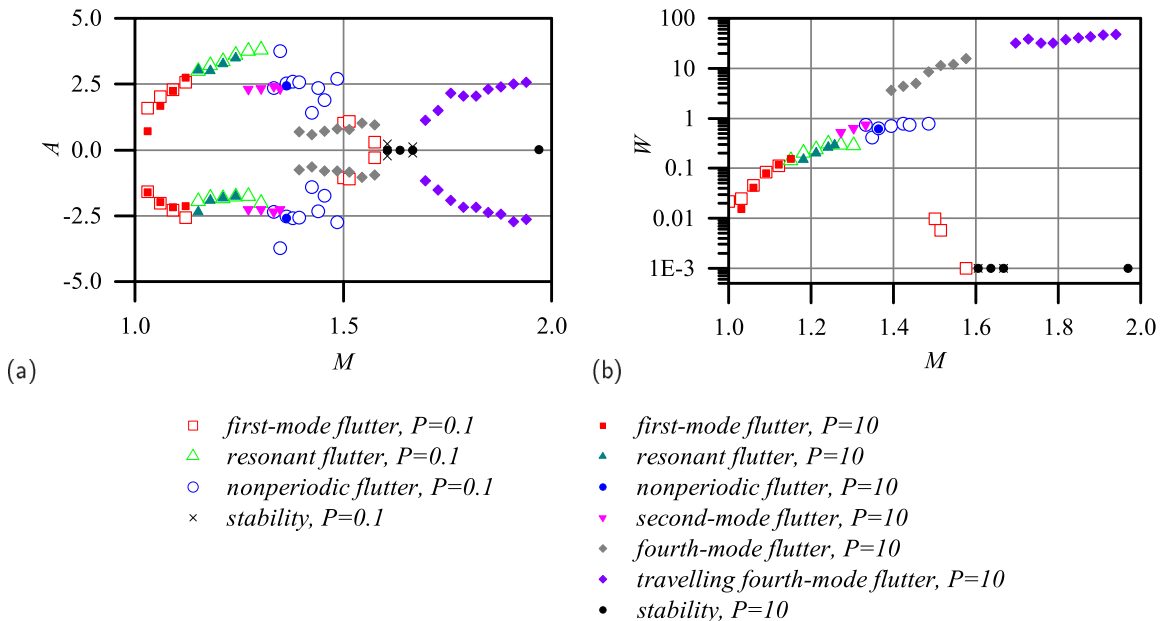


Fig. 12. Amplitude of the control point (a) and energy of the plate (b) under the small ($P = 0.1$) disturbance and strong fourth-mode ($P = 10$) disturbance vs. Mach number.

4.4. The fourth-mode disturbance

Finally, let us consider a strong fourth-mode perturbation (Fig. 12). As before, due to the stability of this mode at lower supersonic Mach numbers and the instability of the first mode, the initial sequence of limit cycles was similar to the previous cases. Namely, the first-mode LCOs occurred at $1 \leq M \leq 1.15$ and the resonant 2:1 LCOs at $1.18 \leq M \leq 1.25$; their amplitude and energy of oscillations were equal to those for the small-amplitude perturbations at $1 < M \leq 1.25$, where the first-mode or resonant LCOs developed. For $1.27 \leq M \leq 1.35$, the second-mode LCOs occurred. This was the same limit cycle as observed after the second-mode initial perturbation; in particular, it has the same amplitude and energy. At an exceptional Mach number $M = 1.37$, non-periodic oscillations occurred, which were similar to those observed at other perturbations.

At larger Mach numbers, the expected fourth-mode oscillations developed. As for the third mode, they were observed in two different forms. Namely, fourth-mode LCOs with a relatively small travelling-wave component developed at $1.39 \leq M \leq 1.57$ (Fig. 13a); for brevity, we will call this regime standing-wave flutter. Then the amplitude sharply decreased almost to zero at $M = 1.6$, and the plate stayed flat up to $M = 1.69$. However, at larger Mach numbers, $1.72 \leq M \leq 1.93$, fourth-mode LCOs developed with much larger travelling-wave component (Fig. 13b), which we will call travelling-wave flutter. This regime had larger amplitude than the standing-wave oscillations. When the standing-wave fourth-mode limit cycle formed at $M = 1.39$, its energy was significantly larger than for previous oscillation regimes. The energy grew with increasing the Mach number until $M = 1.6$. When the travelling-wave oscillations were formed, their

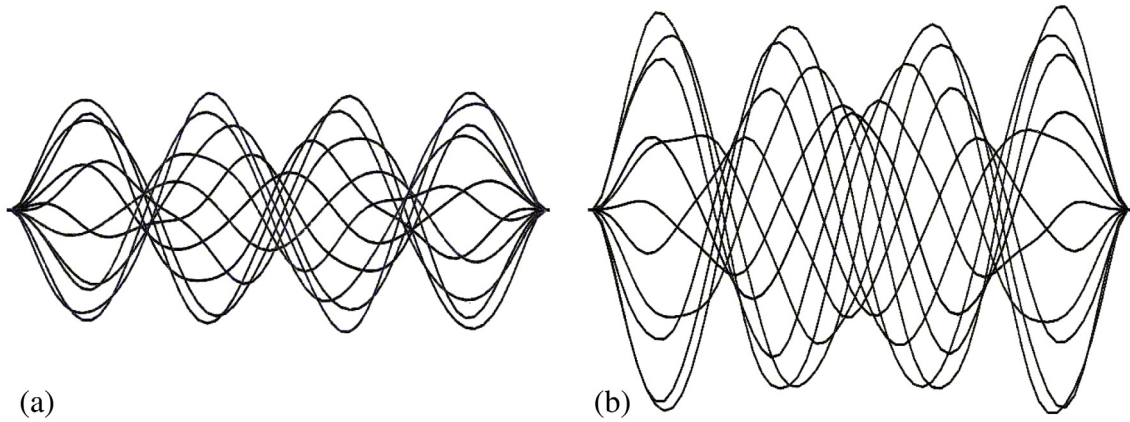


Fig. 13. The plate shape at the fourth-mode flutter in the form of standing wave at $M = 1.42$ (a) and travelling wave at $M = 1.7$ (b) (vertical scale 50:1).

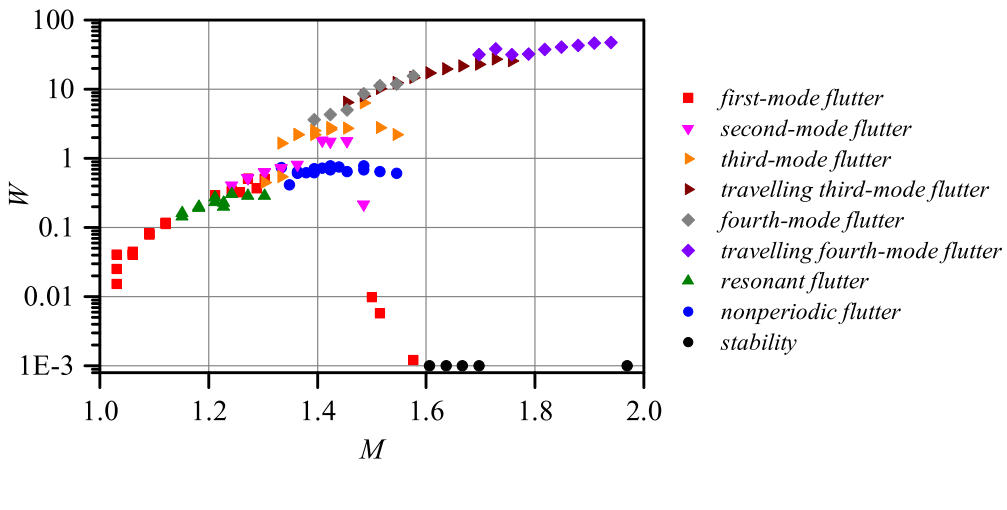


Fig. 14. Energy of the plate under the different modes disturbance vs. Mach number.

energy became significantly larger than of standing-wave oscillations. In terms of the plate energy, the travelling-wave fourth-mode LCOs were the most severe among all observed types of nonlinear oscillations.

4.5. The generalization of the panel response to disturbance in different modes

In this section, we generalize the results obtained by perturbation of various modes (see Fig. 14). Let us divide Mach number range into three segments: $1 \leq M \leq 1.2$, $1.2 \leq M \leq 1.3$, and $1.3 \leq M \leq 2$. There was one branch of the solution at the first segment $1 \leq M \leq 1.2$: first-mode flutter at $1 \leq M \leq 1.12$ and resonant flutter at $1.15 \leq M \leq 1.2$. Next, there were three close branches at the second segment: first-mode flutter, resonant flutter, and second-mode flutter. The second-mode flutter had the highest energy at this segment. Finally, there were seven branches at the last segment $1.3 \leq M \leq 2$: first-mode flutter at $1.54 \leq M \leq 1.7$, second-mode flutter at $1.3 \leq M \leq 1.51$, standing third-mode flutter and nonperiodic flutter at $1.3 \leq M \leq 1.57$, travelling third-mode flutter at $1.45 \leq M \leq 1.75$, standing fourth-mode flutter at $1.39 \leq M \leq 1.57$, and travelling fourth-mode flutter at $1.72 \leq M \leq 1.93$. The first-mode flutter had the lowest energy. The nonperiodic flutter had lower energy than other flutter types except for the first mode. The branches of the fourth-mode flutter and the travelling third-mode flutter were rather close. These types of flutter had the highest energy and were the most dangerous for the plate.

4.6. The effect of the perturbation amplitude

Now, consider the effect of the initial disturbance amplitude on the development of higher-mode oscillations, which are more destructive than the first-mode or resonant LCOs. According to the results discussed above, single-mode limit

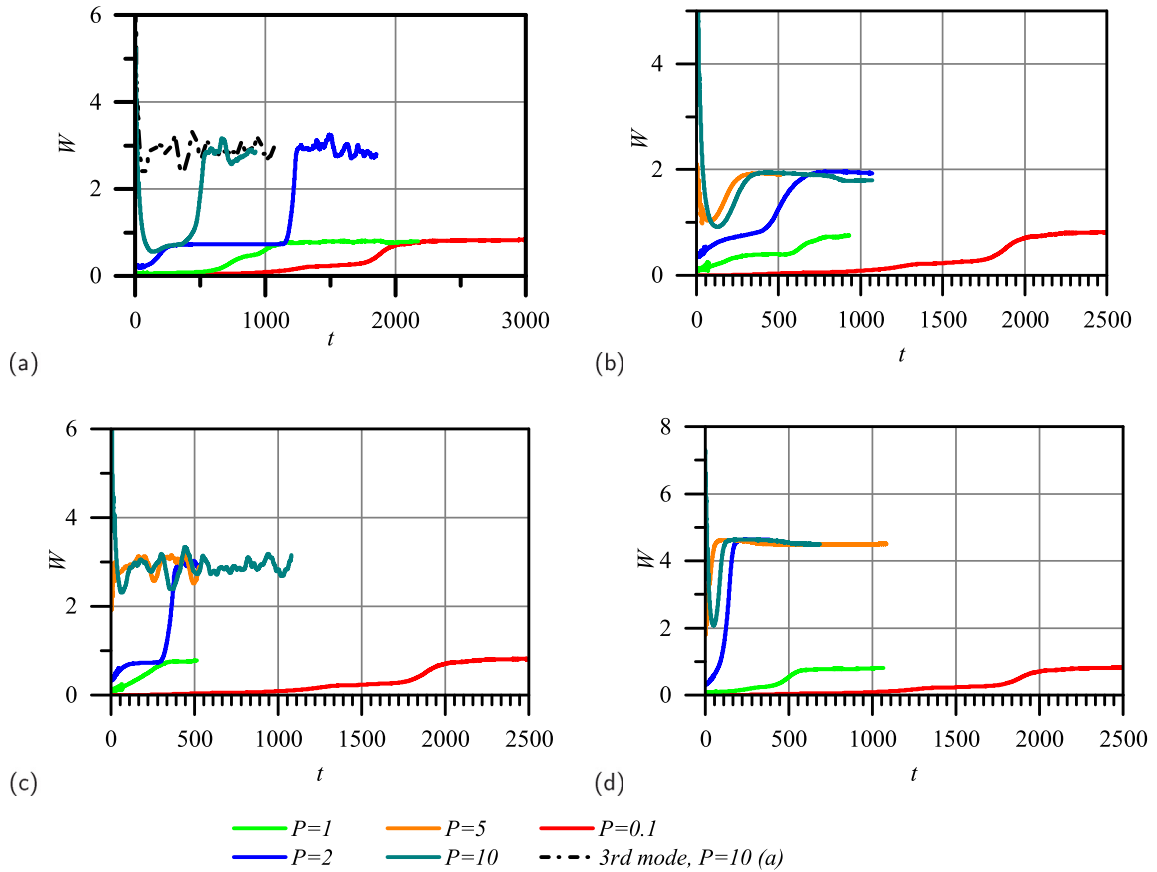


Fig. 15. The plate oscillation energy as a function of time under different amplitudes of the initial perturbation in the form of the first (a), second (b), third (c), and fourth (d) modes at $M = 1.42$.

cycles were excited at $M > 1.22$ by corresponding strong perturbation modes; however, oscillations developed after a small-amplitude perturbation are different. We choose Mach number $M = 1.42$ as representative, at which single-mode limit cycles were observed after the high-amplitude perturbation.

First, consider the first-mode disturbance (Fig. 15a). As shown before, small-amplitude ($P = 0.1$) perturbation yielded nonperiodic oscillations, whereas the strong first-mode disturbance ($P = 10$) initially yielded the same non-periodic oscillations, but then they transformed into the third-mode limit cycle. Fig. 15a also shows results for the third-mode strong perturbation, which evolved into the same limit cycle, whose energy was three times larger than the energy of non-periodic oscillations. Let us also consider ‘intermediate’ amplitudes of the first-mode perturbation with $P = 1$ and $P = 2$. In both cases, the nonperiodic oscillations were developed first, like at $P = 10$ and at $P = 0.1$. While this regime retained at $P = 1$, a larger initial load with $P = 2$ yielded its transformation to the third-mode limit cycle, but much later than for $P = 10$.

Next, consider perturbations in the form of the second, third, and fourth modes (Fig. 15b, c, d). Perturbation amplitudes $P = 1$, $P = 2$, $P = 5$, $P = 10$ were analysed. For the amplitude $P = 1$ or less, the non-periodic oscillations were developed in all cases. For $P = 2$, the same oscillations developed first, but later they transformed into the second- and the third-mode LCOs, except for the fourth-mode perturbations, which evolved into the limit cycle without intermediate non-periodic oscillations. For $P = 5$ and 10 , perturbation evolved onto the corresponding limit cycle immediately, i.e., the stage of non-periodic oscillations was bypassed.

5. The effect of large-amplitude perturbations applied to the plate oscillating in a limit cycle

As demonstrated above, different types of initial perturbation yielded different types of oscillations for the same flow parameters, signifying the existence and stability of multiple limit cycles and the nonperiodic oscillations regime. The higher the oscillation mode, the larger the plate oscillation energy, i.e., larger fatigue damage was accumulated at higher-mode oscillations. Also, the spontaneous transition from nonperiodic oscillations to the third-mode limit cycle was detected. In this section, we analyse, whether it is possible to switch from high-energy to lower-energy LCOs by

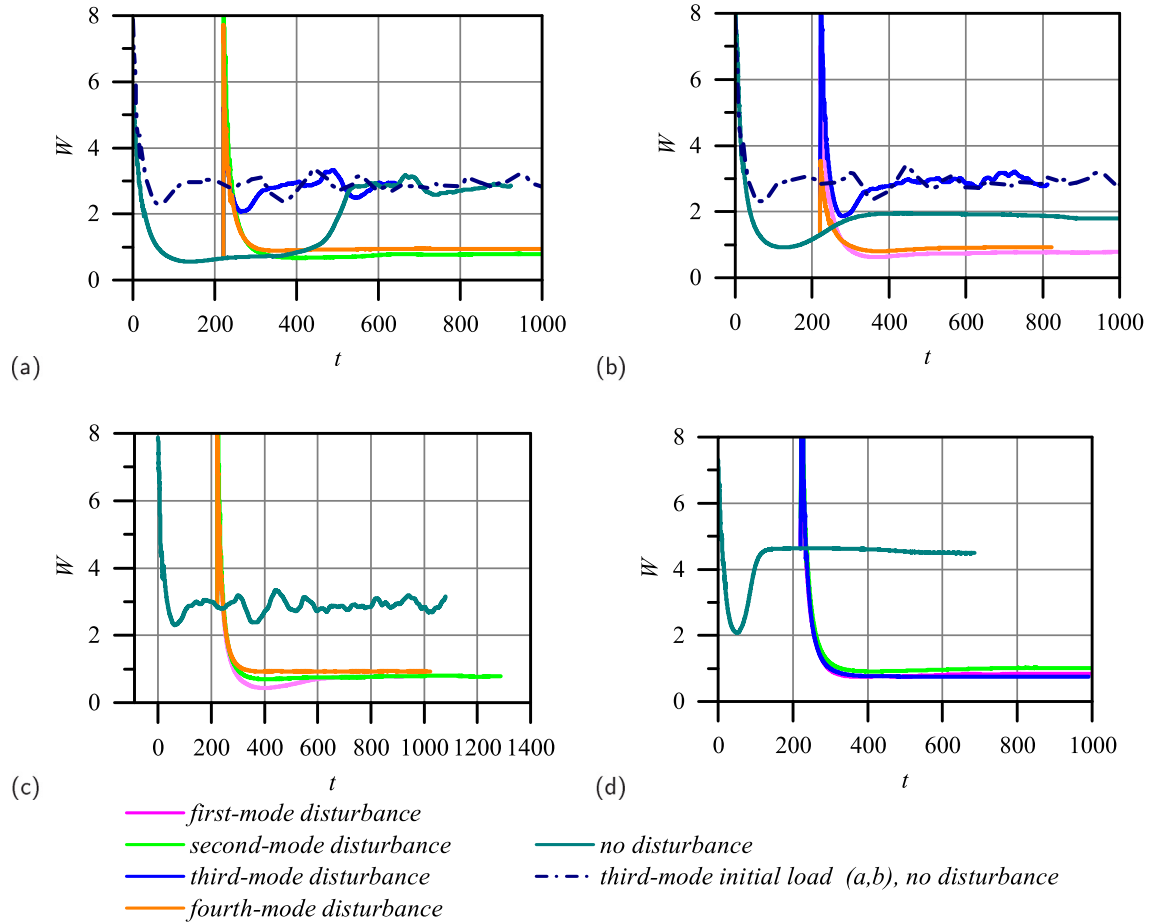


Fig. 16. Plate energy for different modes of secondary disturbance applied to the nonperiodic oscillations (a), the second-mode (b), the third-mode (c) and the fourth-mode (d) LCOs at $M = 1.42$.

applying finite-amplitude perturbations to the oscillating plate. Calculations were conducted after applying an initial strong disturbance with amplitude $P = 10$. After the development of oscillations, at $t = 221$, one more perturbation, also with $P = 10$, was applied to the plate. Calculations showed that the same secondary perturbation as the initial mode could only temporarily increase the energy of oscillations, after which the oscillations were returned to the previous regime. Let us now consider the effect of different-mode secondary perturbation.

5.1. The effect of secondary disturbance at $M = 1.42$

In this section, we consider Mach number $M = 1.42$ as representative, at which various LCOs were observed at different primary perturbations. First, we analysed the effect of the second-, third- and fourth-mode disturbances applied to the nonperiodic oscillations activated by the strong first-mode initial disturbance (Fig. 16a). We observed that the third-mode disturbance led to a fast transformation from the nonperiodic oscillations to the third-mode limit cycle, thus increasing the plate energy by approximately three times. However, the second- and the fourth-mode secondary disturbances did not change the plate dynamics so that non-periodic oscillations were retained.

Next, consider secondary disturbances applied to the second-mode limit cycle oscillations (Fig. 16b). The first-mode and the fourth-mode disturbance transformed the second-mode flutter to the nonperiodic oscillations, the same oscillation regime that developed after the small initial load. As a result of this transformation, the energy of vibration became two times smaller. After the third-mode disturbance, the second-mode LCOs were transformed to the third-mode LCOs. Oscillation energy after this transformation became 1.5 times higher than the energy of the second-mode LCOs.

In the cases of applying secondary disturbance to the third- (Fig. 16c) or fourth-mode LCOs (Fig. 16d), we observed that all types of disturbances transformed original LCOs to nonperiodic oscillations. After this transformation, the oscillation energy became 3 and 4.5 times smaller for the original third- and fourth-mode LCOs, respectively.

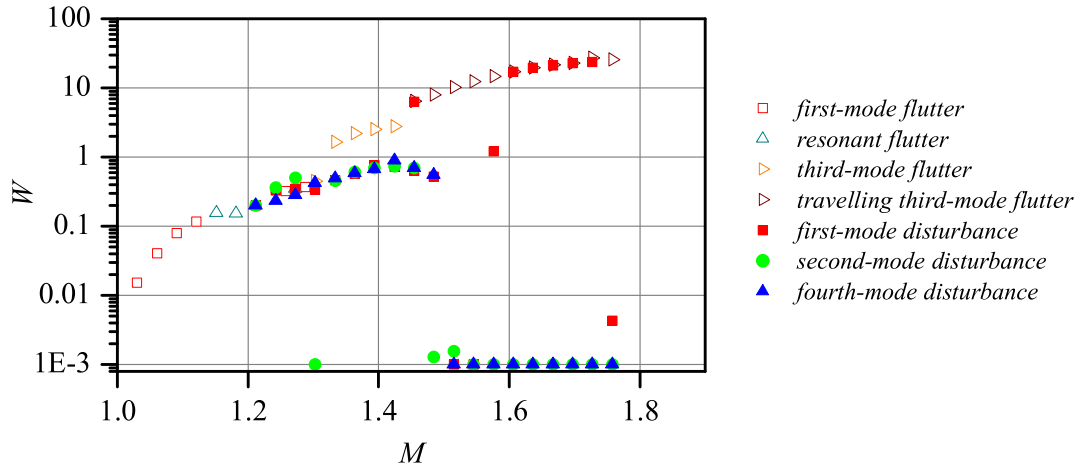


Fig. 17. Energy of plate originally excited by the third-mode strong perturbation, before (empty markers) and after (filled markers) applying the first-, second- and fourth-mode secondary perturbation.

5.2. The effect of secondary disturbance applied to the third-mode LCOs at various Mach numbers

At $M = 1.42$, secondary perturbation of the plate effectively transformed higher-energy limit cycles in the third and fourth modes to lower-energy nonperiodic oscillations, which drastically increased the fatigue lifetime of the plate. We then investigated this effect in a wider range of Mach numbers. We considered the LCOs that appeared under the third-mode initial disturbance at $1.24 \leq M \leq 1.28$ and the third-mode LCOs $1.3 \leq M \leq 1.75$. We did not investigate the secondary perturbation at $M \leq 1.21$, because no effect of the secondary disturbance was observed.

Observation of the oscillating plate shape and energy (Fig. 17) showed that, for the primary first-mode limit cycle at Mach numbers $1.24 \leq M \leq 1.28$, the first-mode and second-mode secondary disturbances transformed any LCOs into the first- and second-mode oscillations, respectively, whereas the fourth-mode disturbance transformed them to the resonant LCOs. For larger Mach numbers, the third-mode LCOs were transformed to the nonperiodic oscillations at $1.3 \leq M \leq 1.48$ and at $M = 1.575$ under the first-mode secondary disturbance, at $1.33 \leq M \leq 1.45$ under the second-mode secondary disturbance, and at $1.33 \leq M \leq 1.48$ under the fourth-mode secondary disturbance. There was no effect of the fourth-mode disturbance at $M = 1.3$. The plate was stabilized (i.e., oscillations disappeared) at $1.51 \leq M \leq 1.54$ under the first-mode disturbance, at $M = 1.3$ and at $1.48 \leq M \leq 1.75$ under the second-mode disturbance, and at $1.51 \leq M \leq 1.75$ under the fourth-mode disturbance. The effect of the first-mode secondary disturbance disappeared at $M > 1.6$: the plate stayed oscillating at the original limit cycle. Also, at $M = 1.45$ dual plate dynamics were observed under the first-mode secondary disturbance: initially, the third-mode limit cycle transformed to the nonperiodic oscillations; then, the latter transformed back to the third-mode limit cycle. In fact, first-mode perturbation did not change the final oscillation regime.

It can be concluded that the second-mode secondary perturbation is the optimal perturbation for the prevention of the most destructive plate oscillations. It either effectively transforms the most energetic limit cycle into lower-energy nonperiodic oscillations, or completely stabilizes the plate. Although the fourth mode has the same effect, its perturbation is dangerous itself, because, if applied with inappropriate amplitude, it can yield oscillations in the travelling-wave fourth-mode limit cycle (Section 4.4), which is even more destructive than the original limit cycle.

6. Discussion and concluding remarks

Single-mode panel flutter is unavoidable for flight vehicles passing or cruising at transonic regime if their panels are not sufficiently damped, because, unlike coupled-mode panel flutter, it occurs at very low dynamic pressures. As was shown in Shishaeva et al. (2018), the most severe high-mode LCOs caused by single-mode flutter can be avoided if the flight vehicle has a large enough acceleration to pass the transonic regime sufficiently quickly. Otherwise, either if the acceleration is low or if the cruise speed is in the transonic regime, as was shown in Shishaeva et al. (2015), different modes of limit cycles oscillations are observed under different initial disturbances at $M > 1.2$; moreover, regions of the existence and stability of different LCOs also vary. For example, results of the present study show that, at $M > 1.51$, the plate stays flat (or flutters with a negligible amplitude) under a small initial disturbance, but LCOs are developed for all four considered types of strong initial disturbance. In other words, strong initial disturbance may be dangerous at Mach numbers that are safe with respect to small-amplitude perturbation. What is more important is that the oscillation energy is significantly larger for higher-mode limit cycles at the same Mach number, which results in a faster accumulation of the fatigue damage. The positive point is that the development of higher-mode LCOs occurs only if the initial perturbation is

sufficiently strong: if its amplitude is lower than a certain value, high-energy limit cycles do not arise, with the exception that the third-mode LCOs can spontaneously develop from non-periodic oscillations, which, in turn, can develop after a small-amplitude perturbation.

We have demonstrated that a strong secondary disturbance, applied to the fluttering panel, can change the type of oscillations. In general, it activates additional mode concurring with the original oscillation mode and yields the transition to non-periodic oscillations, which involve two or more different modes, all being unstable and thus preventing development of a single-mode limit cycle. From a fatigue point of view, this is a preferred regime, because non-periodic oscillations have lower oscillation energy than higher-mode limit cycles, meaning lower strain energy and lower dynamic stress. Again, the only exception is the third-mode LCO spontaneously developed from non-periodic oscillations mentioned above, but, if developed, this high-energy LCO can be destroyed again by a next strong perturbations. We have shown that the second-mode perturbation is the most efficient and safe to destroy high-mode limit cycles. Hence, the results of the present study can be used to design efficient active systems to control panel flutter oscillations.

CRedit authorship contribution statement

Anastasia Shishaeva: Conceptualization, Methodology, Formal analysis, Investigation, Data proceeding, Writing – original draft. **Andrey Aksenov:** Software. **Vasily Vedeneev:** Writing – review and editing, Supervision, Resources.

Declaration of competing interest

The authors declare that they have no known competing financial interests or personal relationships that could have appeared to influence the work reported in this paper.

Funding statement

This work is supported by the Ministry of Science and Higher Education of the Russian Federation within the Programme of “Supersonic” (agreement 075-15-2020-923).

References

- Aksenov, A., Korenev, D., Shishaeva, A., Vucinic, D., Mravak, Z., 2008. Drop-test FSI simulation with abaqus and FlowVision based on the direct 2-way coupling approach. In: 2008 Abaqus Users' Conference, 19–22 May 2008, Newport, Rhode Island (USA): Book of Abstracts. pp. 611–624, URL: https://flowvisioncfd.com/images/articles/2015/Drop-Test_FSI_.pdf.
- Alder, M., 2015. Development and validation of a fluid-structure solver for transonic panel flutter. *AIAA J.* 53 (12), 3509–3521. <http://dx.doi.org/10.2514/1.J054013>.
- Alder, M., 2016. Nonlinear dynamics of pre-stressed panels in low supersonic turbulent flow. *AIAA J.* 54 (11), 3632–3646. <http://dx.doi.org/10.2514/1.J054783>.
- Algazin, S., Kiiko, I., 2006. *Flutter of Plates and Shells*. Nauka, Moscow, p. 360.
- Amabili, M., 2008. *Nonlinear Vibrations and Stability of Shells and Plates*. Cambridge University Press, Cambridge, p. 374.
- Amabili, M., Pellicano, F., 2001. Nonlinear supersonic flutter of circular cylindrical shells. *AIAA J.* 39 (4), 564–573. <http://dx.doi.org/10.2514/2.1365>.
- Amabili, M., Pellicano, F., 2002. Multimode approach to nonlinear supersonic flutter of imperfect circular cylindrical shells. *J. Appl. Mech.* 10, 117–129. <http://dx.doi.org/10.1115/1.1435366>.
- An, X., Qi, B., Sun, W., Deng, B., 2020. Nonlinear single-mode and multi-mode panel flutter oscillations at low supersonic speeds. *J. Sound Vib.* 469, 205–223. <http://dx.doi.org/10.1016/j.jfluidstructs.2015.05.005>.
- Bendiksen, O., Davis, G., 1995. Nonlinear traveling wave flutter of panels in transonic flow. In: *AIAA Paper-95-1486*, p. 17. <http://dx.doi.org/10.2514/6.1995-1486>.
- Bhatia, M., Beran, P., 2018. Influence of aerodynamic nonlinearity due to static panel-curvature on flutter of panels at transonic and low supersonic mach numbers. *J. Fluids Struct.* 81, 574–597. <http://dx.doi.org/10.1016/j.jfluidstructs.2018.05.015>.
- Bolotin, V., 1963. *Nonconservative Problems of the Theory of Elastic Stability*. Pergamon Press, Oxford, p. 324.
- Bondared, V., Vedeneev, V., 2016. Short-wave instability of an elastic plate in supersonic flow in the presence of the boundary layer. *J. Fluid Mech.* 802, 528–552. <http://dx.doi.org/10.1017/jfm.2016.482>.
- Bondared, V., Vedeneev, V., 2017. Flutter of infinite elastic plates in the boundary-layer flow at finite Reynolds numbers. *Fluid Dyn.* 52 (6), 797–814. <http://dx.doi.org/10.1134/S0015462817060040>.
- Bondared, V., Vedeneev, V., 2018. Influence of the viscous boundary layer perturbations on single-mode panel flutter at finite Reynolds numbers. *J. Fluid Mech.* 852, 578–601. <http://dx.doi.org/10.1017/jfm.2018.527>.
- Boyer, N.R., McNamara, J., Gaitonde, D., Barnes, C.J., Visbal, M.R., 2018. Features of shock-induced panel flutter in three-dimensional inviscid flow. *J. Fluids Struct.* 83, 490–506. <http://dx.doi.org/10.1016/j.jfluidstructs.2018.10.001>.
- Budiansky, B., Sanders, J.J., 1962. On the “Best” First-Order Linear Shell Theory. Technical report No. 14, Office of Naval Research.
- Dassault Systèmes, 2012. *Abaqus Theory Manual*, Vol. 6.12. Dassault Systèmes.
- Dowell, E., 1967. Nonlinear oscillations of fluttering plate. II. *AIAA J.* 5 (10), 1856–1862. <http://dx.doi.org/10.2514/3.4316>.
- Dowell, E., 1973. Aerodynamic boundary layer effect on flutter and damping of plates. *J. Aircr.* 10 (12), 734–738. <http://dx.doi.org/10.2514/3.60298>.
- Dowell, E., 1975. *Aeroelasticity of Plates and Shells*. Nordhoff International Publishing, Leyden, p. 153.
- Gaspers, P.A.J., Jr., M.L., N., P.D., 1970. Further Experimental Results on the Influence of the Turbulent Boundary Layer on Panel Flutter. NASA TN D-5798, URL: <https://core.ac.uk/download/pdf/80657219.pdf>.
- Gordnier, R., Visbal, M., 2002. Development of a three-dimensional viscous aeroelastic solver for nonlinear panel flutter. *J. Fluids Struct.* 16 (4), 497–527. <http://dx.doi.org/10.1006/jfls.2000.0434>.
- Grigolyuk, E., Lamper, R., Shandarov, L., 1965. Flutter of plates and shells. In: *Itogi Nauki. Mekhanika*. VINITI, Moscow, pp. 34–90.

- Hashimoto, A., Aoyama, T., Nakamura, Y., 2009. Effect of turbulent boundary layer on panel flutter. *AIAA J.* 47 (12), 2785–2791. <http://dx.doi.org/10.2514/1.35786>.
- Hejranfar, K., Azampour, M., 2016. Simulation of 2D fluid-structure interaction in inviscid compressible flows using a cell-vertex central difference finite volume method. *J. Fluids Struct.* 67, 190–218. <http://dx.doi.org/10.1016/j.jfluidstructs.2016.09.009>.
- Mei, C., Abdel-Motagaly, K., Chen, R., 1999. Review of nonlinear panel flutter at supersonic and hypersonic speeds. *Appl. Mech. Rev.* 69, 321–332. <http://dx.doi.org/10.1115/1.3098919>.
- Mei, G., Zhang, J., Kang, C., 2017. Analysis of curved panel flutter in supersonic and transonic airflows using a fluid-structure coupling algorithm. *J. Vib. Acoust.* 139 (4), <http://dx.doi.org/10.1115/1.4036103>.
- Mei, G., Zhang, J., Xi, G., Sun, X., Chen, J., 2014. Analysis of supersonic and transonic panel flutter using a fluid-structure coupling algorithm. *J. Vib. Acoust.* 136, 031013. <http://dx.doi.org/10.1115/1.4027135>.
- Muhlstein, L.J., Gaspers, P.A.J., Riddle, D.W., 1968. An Experimental Study of the Influence of the Turbulent Boundary Layer on Panel Flutter. NASA TN D-4486, URL: <https://ntrs.nasa.gov/api/citations/19680009252/downloads/19680009252.pdf>.
- Novichkov, Y., 1978. Flutter of plates and shells. In: *Progress in Science and Technology. In: Mechanics of Deformable Solids, vol. 11*, VINITI, Moscow, pp. 67–122.
- Shinde, V., McNamara, J., Gaitonde, D., Barnes, C., Visbal, M., 2019. Transitional shock wave boundary layer interaction over a flexible panel. *J. Fluids Struct.* 90, 263–285. <http://dx.doi.org/10.1016/j.jfluidstructs.2019.07.007>.
- Shishaeva, A., Vedeneev, V., Aksenov, A., 2015. Nonlinear single-mode and multi-mode panel flutter oscillations at low supersonic speeds. *J. Fluids Struct.* 56, 205–223. <http://dx.doi.org/10.1016/j.jfluidstructs.2015.05.005>.
- Shishaeva, A., Vedeneev, V., Suskho, G., Aksenov, A., 2018. Transonic panel flutter in accelerating or decelerating flow conditions. *AIAA J.* 56 (3), 997–1010. <http://dx.doi.org/10.2514/1.J056217>.
- Shitov, S., Vedeneev, V., 2017. Flutter of rectangular simply supported plates at low supersonic speeds. *J. Fluids Struct.* 69, 154–173. <http://dx.doi.org/10.1016/j.jfluidstructs.2016.11.014>.
- Vedeneev, V., 2007. Nonlinear high-frequency flutter of a plate. *Fluid Dyn.* 5, 858–868. <http://dx.doi.org/10.1134/S0015462807050183>.
- Vedeneev, V., 2012. Panel flutter at low supersonic speeds. *J. Fluids Struct.* 29, 79–96. <http://dx.doi.org/10.1016/j.jfluidstructs.2011.12.011>.
- Vedeneev, V., 2013a. Effect of damping on flutter of simply supported and clamped panels at low supersonic speeds. *J. Fluids Struct.* 40, 366–372. <http://dx.doi.org/10.1016/j.jfluidstructs.2013.04.004>.
- Vedeneev, V., 2013b. Interaction of panel flutter with inviscid boundary layer instability in supersonic flow. *J. Fluid Mech.* 736, 216–249. <http://dx.doi.org/10.1017/jfm.2013.522>.
- Vedeneev, V., 2013c. Limit oscillatory cycles in the single mode flutter of a plate. *J. Appl. Math. Mech.* 77 (3), 257–267. <http://dx.doi.org/10.1016/j.jappmathmech.2013.09.001>.
- Vedeneev, V., Nesterov, V., 2019. Effect of nonequilibrium reacting flow on flutter at hypersonic flight speed. *AIAA J.* 57 (5), 2222–2226. <http://dx.doi.org/10.2514/1.J057713>.
- Visbal, M., 2013. Viscous and inviscid interactions of an oblique shock with a flexible panel. *J. Fluids Struct.* 48, 27–45. <http://dx.doi.org/10.1016/j.jfluidstructs.2014.02.003>.
- Willems, S.A., Gülhan, A., Esser, B., 2013. Shock induced fluid-structure interaction on a flexible wall in supersonic turbulent flow. *Prog. Flight Phys.* 5, 285–308. <http://dx.doi.org/10.1051/eucass/201305285>.
- Zhou, H., Wang, G., Mian, H.H., Qin, M., 2021. Fluid-structure coupled analysis of tandem 2D elastic panels. *Aerosp. Sci. Technol.* 111, 106521. <http://dx.doi.org/10.1016/j.ast.2021.106521>.